



# 11<sup>th</sup> International Seminar on Inland Waterways and Waterborne Transportation

Brasília/DF, 22th to 24th October 2019

## Parametric Analysis of Welding Parameters for Hybrid Laser/MAG Welding

Shuichi Tsumura, NMRI, Tóquio/Japão, [tsumura-s@nmri.go.jp](mailto:tsumura-s@nmri.go.jp)

Eduardo Meirelles, UFRJ/COPPE, Rio de Janeiro/Brasil, [eduardomeirelles@oceanica.ufrj.br](mailto:eduardomeirelles@oceanica.ufrj.br)

Victor Mello Callil, UFRJ/COPPE, Rio de Janeiro/Brasil, [mellov96@poli.ufrj.br](mailto:mellov96@poli.ufrj.br)

Marcelo Igor Lourenço, UFRJ/COPPE, Rio de Janeiro/Brasil, [migor@lts.coppe.ufrj.br](mailto:migor@lts.coppe.ufrj.br)

Jean-David Caprace, UFRJ/COPPE, Rio de Janeiro/Brasil, [idcaprace@oceanica.ufrj.br](mailto:idcaprace@oceanica.ufrj.br)

### Abstract

*Fusion welding is a largely applied method in naval industry, which enables structural strength and watertightness between joined parts. Distinct welding processes were developed, granting various advantages as productivity, structural strength and possibility to join thicker plates. The combination of different welding processes tends to overcome some particular disadvantages of each one, as seen in hybrid laser/GMAW welding. However, the resultant state of the welded structure becomes more complex to predict, as the possible combinations of welding parameters grows severely on hybrid welding. The purpose of the present work is to evaluate how is affected the behaviour of weld beads and welded structures when hybrid welding parameters are varied. Experimentally, a set of hybrid laser/MAG welds were performed on KD36 (NK Grade), combining different values of laser power, MAG voltage and amperage, travel speed and plate thickness. Temperature field, weld bead dimensions, hardness and residual stresses were the main collected data. For the simulations were carried two combinations of heat sources, where MAG welding was set as a double ellipsoid and laser as a double ellipsoid and a cylindrical heat source. Were observed that the heat input of each welding process influences with different weights the weld bead dimensions. For the parameters evaluated, hardness presented standard behaviour with higher values at FZ and HAZ. Therefore, these regions are more susceptible to break down when submitted to high loads. The simulations achieved a good agreement with measured residual stresses, showing that both combinations of heat sources are efficient.*

### 1. Introduction

Naval structures are requiring a good design in terms of resistance, reliability and safety. Normally, shipbuilding industry uses thick plates in the bottom and the main deck to ensure that the structure will support the loads and corrosion during their operating life.

In this background, welding of thick plates became a laborious task. It is generally carried out using multiple passes of gas metal arc welding (GMAW) or submerged arc welding (SAW). These traditional processes present some shortcomings like local distortions, high heat input, extensive time for bevel preparation, long welding time and necessity of many passes in one joint. In the other hand, laser welding allows deep penetration, low heat input and single-pass weld bead. However, it

demands a quite precise gap between the workpieces. This requirement is tough to achieve depending on the shipyard.

Recently, there have been significant advances in the development of high-power laser and gas metal arc welding (GMAW), known as hybrid welding. The addition of an arc welding to the laser process allowed a lower precision in terms of machining of the workpieces and rose up welding speed. Such considerations made hybrid laser as a promising technology in shipbuilding providing many advantages such as deep penetration, single-pass weld and greater fit tolerance of the workpieces; (M.Wahba, et al., 2016) and (Pan, et al., 2016).

As far as hybrid process has being applied over the past few years, the necessity of a better evaluation

in terms of thermal cycle grows, as well as the deformation and residual stress. Ma *et al.* (2015) investigated the effect of energy ratio on a hybrid welded SS400 butt joint profile in terms of deformation and residual stress with experimental and numerical simulations method. It was found that the energy ratio leads to significant residual stress that influences the bending and shrinkage in longitudinal and transverse directions. (Kong, et al., 2011) approached a thermo-mechanical finite element model to predict the temperature influence on the residual stress led by hybrid laser-GMAW welding process. The heat source is assumed to be a double-ellipsoid heat source presented by Goldak (1984). It is concluded that temperature variation had a great influence on the formation and quality of weld bead. Piekarska and Kubiak (2011) used numerical analysis to predict temperature along the welding zones. The numerical results include the velocity field of liquid material and the temperature field. The heat source was also modelled according to Goldak's model.

For many applications of hybrid laser-arc welding, traditional techniques to predict residual stress in steel plates have been an open problem. The lack of more robust investigations limits the application of hybrid laser in terms of material and stress requirements depending on region of the vessel structure.

In this paper, we describe a comparison between experiment and numerical results to predict residual stress for different process parameters using hybrid laser-arc welding. The heat source was modelled as a combination of Goldak's and cylindrical heat sources, leading the simulation to consistent temperature distribution and residual stresses prediction.

## 2. Welding Experiment

Hybrid Laser Beam Welding (HLBW) is a combination of a laser beam welding with an electrical arc welding. For the project was adopted the Gas Metal Arc Welding (GMAW). This combination tries to join the main advantages of each method. Laser weld has a great penetration at high speeds, which may not be achieved by a single pass of GMAW. However, laser welding does not generate reinforcement on the weld bead, as it is not used a filler material. Therefore, GMAW may be useful to overcome this advantage.

A scheme of the hybrid welding is presented in Figure 1. It is possible to note the difference in

penetration generated by each welding method, where laser beam reaches greater depths. The main parameters that will determine the penetration are laser power and travel speed. GMAW power and travel speed will be significant on the width and reinforcement of the weld. It is possible to weld on both welding directions, having the laser beam on the leading side or the GMAW. Another important feature is the shielding gas that will affect the weld characteristics, as it may be an active or inert gas.

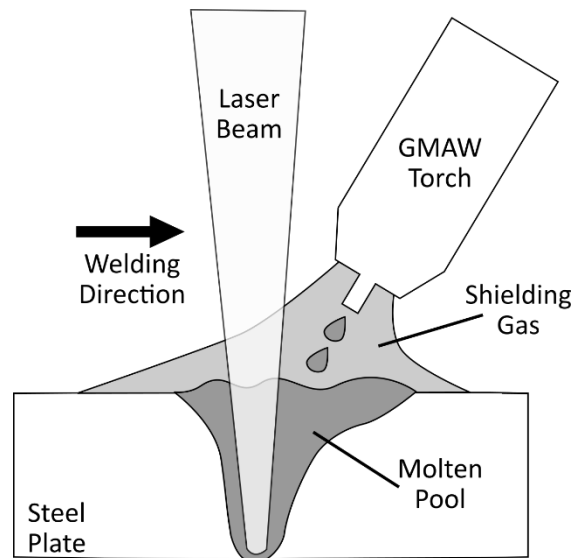


Figure 1 - Hybrid Laser/GMAW welding scheme

### 2.1. Experimental Setup

The focuses of the present study are linked to the temperature distribution for butt weld. Therefore, the experiments were made with a single plate of steel without bevel. This is possible due to the laser beam welding, which do not use filler material. Moreover, the GMAW function is to generate the reinforcement, not primarily interfered by the presence of a bevel. The dimensions of the plate are 300 x 200 mm, varying the thickness by each experiment.

For some experiments, thermocouples were positioned near the welding line in order to capture the temperature variation during welding. Six thermocouples were attached as presented in Figure 2, centred in longitudinal direction and spacing 30 mm for each group. On the transversal direction, the thermocouples located at point 1, point 3, and point 5 distance 15 mm from the welding line, and the thermocouples located at point 2, point 4, and point 6 distance 20 mm from the welding line

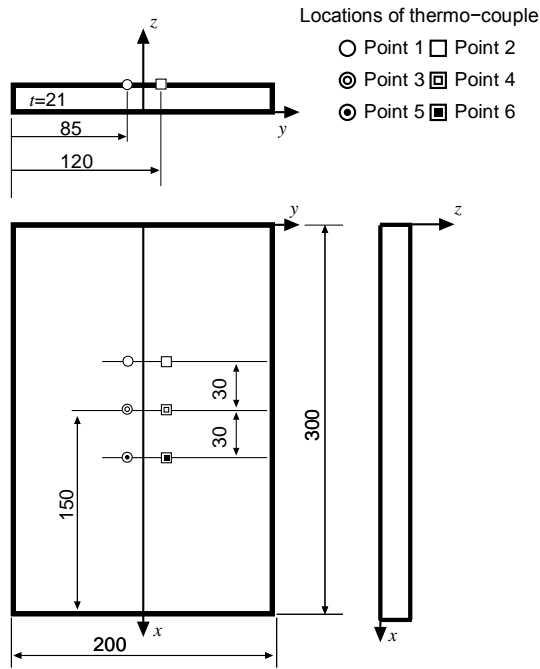


Figure 2 - Thermocouples configuration

The steel used on the experiments is the KD36 (NK Grade), which composition is presented in Table 1.

Table 1 - Standard value of chemical composition of KD36 steel (Wt %)

C	Si	Mn	P	S
Less than 0.18	Less than 0.5	0.9 to 1.6	Less than 0.035	Less than 0.035

32 experiments were carried out, 16 in the first run and 16 on the second. Different combinations of laser and GMAW power, travel speed and plate thickness were adopted. Laser has been varied from 3 to 9 kW and GMAW from 4 to 9 kW. Travel speed started at 0.5 m/min going to 1.1 m/min. The minimum plate thickness was 7 mm and the maximum 21 mm. The configuration for each experiment is presented in Table 2 and Table 3. The used shielding gas was  $CO_2$ .

## 2.2. Measurements

As exposed before, the experiments were set with thermocouples in order to record the thermal history during welding. These data are important to define the parameters of the equivalent heat source, which is crucial to perform welding simulations.

The second measurements that were made are the characteristics of each weld profile. Figure 3 shows the features that had been measured using micrographs. Three dimensions were assessed on

the fusion zone (FZ), the width on the surface of the plate, the depth from the surface to the bottom and the height, given by the distance from the top of reinforcement to the bottom. Moreover, the areas of superior fusion zone, inferior fusion zone and heat affected zone (HAZ) were measured.

Table 2 - Welding configuration for the first run

ID	Thickness [mm]	Travel Speed [m/min]	Laser Power [kW]	GMAW Power [kW]
1	17	0.8	5	5
2	7	1.0	4	5
3	17	1.1	5	4
4	7	1.1	4	7
5	14	0.7	8	5
6	14	0.9	6	8
7	14	0.8	5	5
8	14	0.9	5	7
9	17	1.0	8	7
10	17	0.8	7	6
11	17	0.8	9	5
12	17	0.6	6	8
13	21	0.5	9	5
14	21	0.6	8	9
15	21	1.1	9	8
16	21	0.9	9	9

Table 3 - Welding configuration for the second run

ID	Thickness [mm]	Travel Speed [m/min]	Laser Power [kW]	GMAW Power [kW]
17	7	1.1	3	5
18	7	0.9	3	5
19	7	1.0	3	5
20	7	1.1	4	4
21	7	0.9	4	4
22	7	1.1	4	5
23	7	0.9	4	5
24	7	1.0	4	7
25	7	1.1	5	4
26	7	0.9	5	4
27	7	1.1	5	5
28	7	0.9	5	5
29	7	1.0	5	5
30	7	1.1	6	4
31	7	0.9	6	4
32	7	1.0	6	4

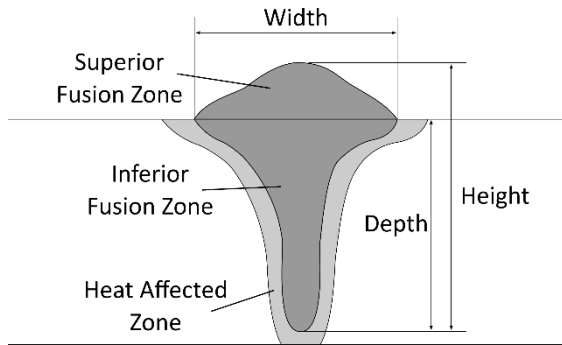


Figure 3 – Measured features of the weld bead profile

The last assessed data are the residual stresses, which was used to evaluate the results of the simulation. These stresses were measured by the X ray diffraction  $\text{Cos}\alpha$  Method using the PULSTEC- $\mu\text{X}360$ .

Microhardness was carried out according to DNVGL-ST-F101 (2017). The rule recommends to use different distance of indentation depending on the weld region. In the top, the distance should be around 1 mm at FZ, 0.5-1.0 mm at HAZ and 0.5 – 1.5 mm at PM. In the middle and the root, the distance decreases because the weld zone is narrower. The distances are shown in Figure 4, provided by DNV Rule.

In order to evaluate the effect of different parameters and thickness on the weld properties, ID's 6, 11, 13 and 16 were selected. In the top, three indentations were made 1.0 mm apart from each other at FZ; the HAZ underwent four indentations 500  $\mu\text{m}$  apart from each other while PM was submitted to three indentations 1.0 mm apart. In the middle, FZ and HAZ had three each with indentations 250  $\mu\text{m}$  distant from each other; PM had three indentations 500  $\mu\text{m}$  apart. After test, two charts were plotted to compare the hardness of ID's 6, 11, 13 and 16 in the top and the middle.

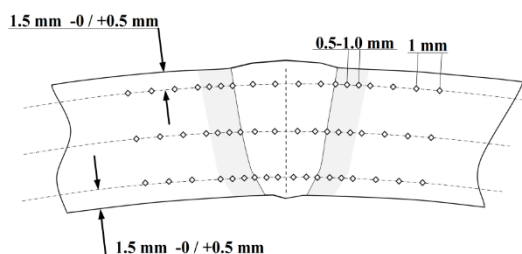


Figure 4 - Recommended distance in FZ, HAZ and PM for non-clad samples by DNVGL-ST-F101

### 3. Welding Simulation

Simulations gained an important role in prediction of welding consequences, as residual stresses and distortions. Derakhshan (2018), Pasternak (2017) and Xia (2018) are authors that shows the currently welding simulation capacity for the assessment of residual stresses, which are the aim of the present work. Next are presented the modelling and considerations made for the simulation of experiment ID14.

#### 3.1. FE Modelling

A thermo-elasto-plastic simulation was carried for experiment ID14 considering only half of the work piece. As the studied structure is symmetric over the weld line, this technique decreases the necessary computational effort. The model was meshed using 8-node isoparametric elements, adopting a minimum element size of 0.875 mm, 1.5 mm and 1.0 mm. Figure 5 presents the prepared model.

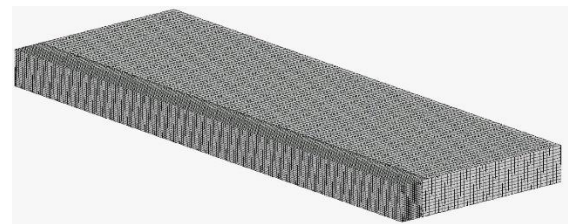


Figure 5 - FE modelling of half model of butt-joint

#### 3.2. Material Properties

The used values for physical and mechanical properties were given by Mochizuki *et al.* (1995) and Kim *et al.* (2005), respectively. Pardo *et al.* (1989) studied the influence of phase change to consider the thermal conductivity of the liquid phase. As a result, when the thermal conductivity was set for 5 times just before the liquid phase values, the estimation and experimental data showed good agreement. Therefore, in FE analysis, the value of thermal conductivity was set 5 times the reference value when the temperature is more than 1500 degree Celsius. The physical contents are shown in Figure 6 and mechanical properties in Figure 7.

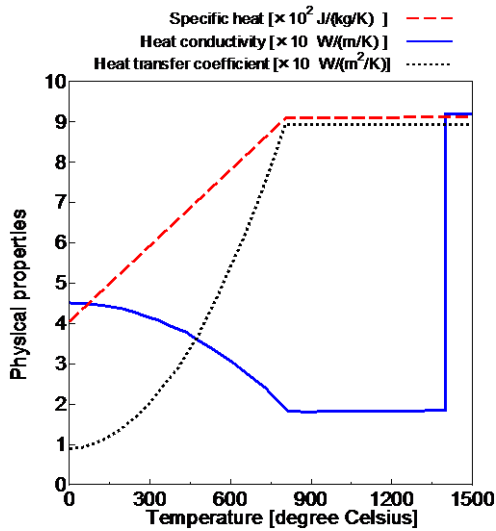


Figure 6 - Physical properties by temperature

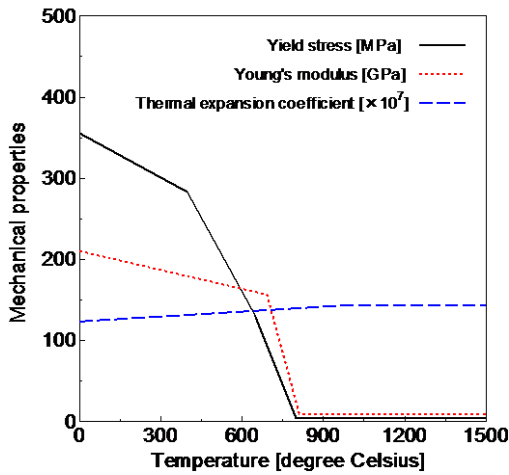


Figure 7 - Mechanical properties by temperature

### 3.3. Equivalent Heat Source

One of the most important procedures of a welding simulation is the adjustment of the heat source. It defines how the heat will spread over the base plate and the temperature field evolve. Due to the great difference of fusion zones generated by each welding method in hybrid welding, it is necessary to combine two heat sources for a simulation. One heat source for each welding method. For this project, were evaluated two combinations of heat sources as presented next in Table 4.

Combination	Laser	GMAW
Cylindrical Combination	Cylindrical	Double Ellipsoid
Double Ellipsoid Combination	Double Ellipsoid	Double Ellipsoid

The first combination is composed by a cylindrical heat source for the laser beam and a double ellipsoid for the GMAW. This combination will be called cylindrical combination. For the second combination the cylindrical heat source of the laser beam is changed to a double ellipsoid heat source, which will be called double ellipsoid combination. Cylindrical heat source is mainly defined by two parameters,  $r$  and  $h$ , which are the radius and the height, respectively. Moreover, it is used a  $\alpha$  parameter, defining the how the heat is distributed over the height. For  $\alpha = 0$ , the heat is constant over the height. For  $\alpha = 1$ , the heat on the top is  $q_c = 2Q/V$  and  $q_c = 0$  on the bottom. As needed for all heat sources, it is also defined the heat flux ( $Q$ ) and the efficiency. Figure 8 shows the cylindrical heat source scheme.

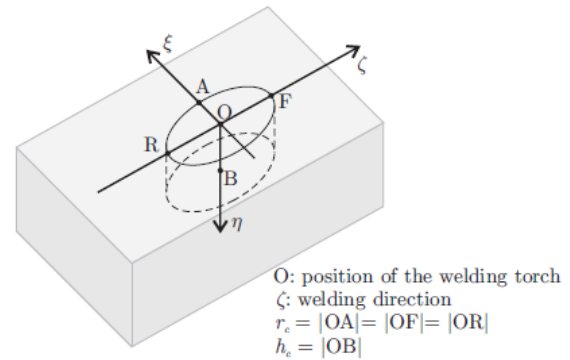


Figure 8 - Cylindrical heat source, defined by the parameters  $r$  and  $h$

The heat distribution for the cylindrical heat source is given by:

$$q_c(\xi, \eta, z) = \begin{cases} \frac{2Q}{(2-\alpha)V} \left(1 - \alpha \frac{|\eta|}{h}\right), & \text{if } \xi^2 + z^2 \leq r^2 \\ 0, & \text{otherwise} \end{cases}$$

The double ellipsoid heat source, also called Goldak (1984) heat source, is the combination of two volumetric ellipsoids. Depicted in Figure 9, it is defined by four parameters. The length of the front part given by  $a_f$ , the rear part given by  $a_r$ , the width is equal to  $b$  and the depth given by  $c$ . As needed for all heat sources, it is also defined the heat flux ( $Q$ ) and the efficiency.

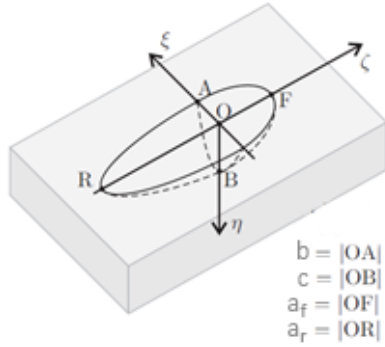


Figure 9 - Double ellipsoid heat source, defined by the parameters  $a_f$ ,  $a_r$ ,  $b$  and  $c$

The heat distribution for the double ellipsoid heat source is given by:

$$q_i(\xi, \eta, \zeta) = \frac{6\sqrt{3} f_i \eta Q}{bc a_i \pi \sqrt{\pi}} \exp\left(-\frac{3\xi^2}{b^2} - \frac{3\eta^2}{c^2} - \frac{3\zeta^2}{a_i^2}\right)$$

Where the index  $i$  is equal to  $f$  or  $r$ , defining the front or rear part of the double ellipsoid, respectively.

As exposed earlier, the heat sources are adjusted using the thermal history obtained by the thermocouples. Currently, the method to obtain the parameters of the equivalent heat source is based on trial and error. These parameters are obtained simulating from a starting set of heat sources and being refined until reach the experimental thermal history. For the experiment 14, the set of parameters for the cylindrical combination is given in Table 5 and Table 6. The same procedure was made for the double ellipsoid combination and was possible to maintain the GMAW heat source parameters. The double ellipsoid for the laser beam is given in Table 7.

Table 5 - Cylindrical heat source parameters for laser welding

Q	Efficiency	$\alpha$	$r$	$h$
[kW]	[-]	[-]	[mm]	[mm]
8000	0.7	0.9	0.5	16

Table 6 - Double ellipsoid heat source parameters for GMAW welding

Power	Efficiency	$a_f$	$a_r$	$b$	$c$
[kW]	[-]	[mm]	[mm]	[mm]	[mm]
9000	0.7	2	6	7	2

Table 7 - Double ellipsoid heat source parameters for laser welding

Power	Efficiency	$a_f$	$a_r$	$b$	$c$
[kW]	[-]	[mm]	[mm]	[mm]	[mm]
8000	0.7	0.5	0.5	0.5	20

Figure 10 and Figure 11 show the thermal development for the experiment and the simulation. It is possible to note that the defined parameters for the cylindrical and double ellipsoid combinations are in good agreement with the experiment.

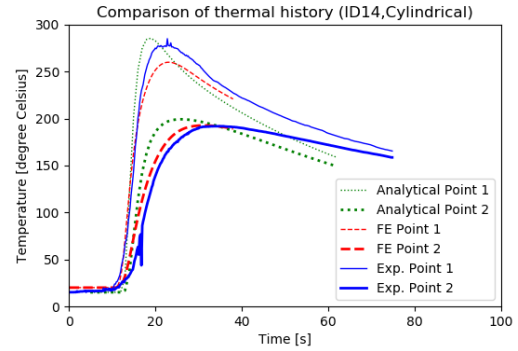


Figure 10 - Comparison of the experiment and simulation thermal history for the cylindrical combination

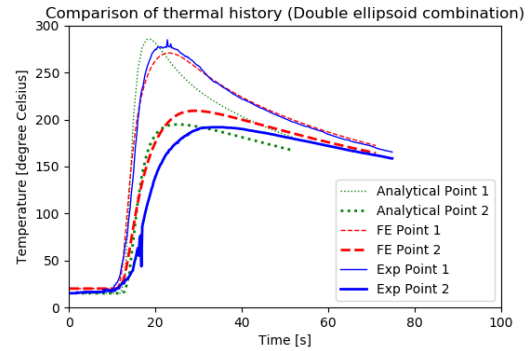


Figure 11 - Comparison of the experiment and simulation thermal history for double ellipsoid combination

## 4. Results and Discussion

### 4.1. Experimental Results

The experimental part of the project was concerned to measure the generated fusion and heat affected zones for each experiment. Using a micrography of the weld bead was possible to delimitate these zones and collect the data. An example of a used micrography is presented in Figure 12, showing the contour of fusion and heat affected zones. Is also depicted the width, depth and height of the weld bead.

The results for each experiment are presented next, where Table 8 and Table 9 bring the dimensions of fusion zone for first and second runs, respectively. For the fusion and heat affected zones, Table 10 and Table 11 contain the areas of

superior and inferior fusion zone and heat affected zone.

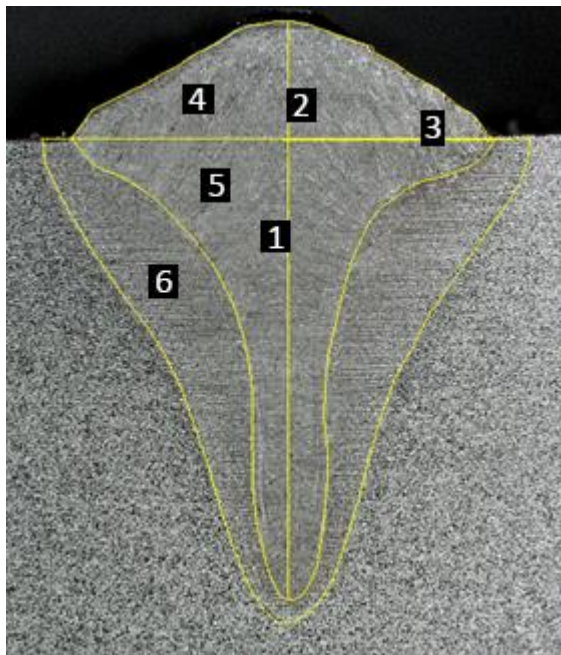


Figure 12 - Example of a studied micrograph (ID1), highlighting dimensions and shape of fusion and heat affected zones. 1-Depth. 2-Height. 3-Width. 4-Superior Fusion Zone. 5-Inferior Fusion Zone. 6-Heat Affected Zone

Table 8 - Molten pool shape for the experiments of the first run

ID	Width (mm)	Height (mm)	Depth (mm)
1	6.9	9.5	7.6
2	6.1	7.7	6.0
3	5.8	7.6	6.3
4	7.2	7.6	5.4
5	9.2	14.7	12.5
6	8.6	12.1	10.1
7	8.0	9.5	7.5
8	7.7	10.4	8.2
9	8.5	12.8	11.0
10	8.2	13.6	11.3
11	7.8	14.8	12.8
12	10.8	14.1	11.6
13	10.9	17.6	15.4
14	11.9	16.8	14.2
15	8.6	13.4	11.6
16	9.6	16.4	14.2

Table 9 - Molten pool shape for the experiments of the second run

ID	Width (mm)	Height (mm)	Depth (mm)
17	4.9	5.0	2.9
18	5.6	5.3	2.9
19	3.9	5.4	3.0
20	4.2	6.8	4.6
21	4.6	7.0	4.8
22	4.7	6.6	4.4
23	4.7	7.2	5.0
24	5.8	7.9	5.1
25	3.9	6.9	5.5
26	5.3	8.5	6.4
27	5.5	8.2	5.9
28	5.7	8.2	5.8
29	5.5	8.7	6.2
30	5.6	7.9	5.7
31	6.3	8.5	6.4
32	6.2	8.8	6.4

Table 10 - Molten pool areas for the experiments of the first run

ID	FZ Inf Area (mm <sup>2</sup> )	FZ Sup Area (mm <sup>2</sup> )	HAZ Area (mm <sup>2</sup> )
1	15.6	8.3	32.5
2	10.5	6.8	24.3
3	11.4	4.5	22.1
4	13.8	9.8	23.8
5	30.7	11.8	61.1
6	23.3	10.1	52.6
7	17.2	10.0	38.2
8	17.9	10.5	38.2
9	24.5	8.7	56.1
10	24.1	10.7	59.0
11	27.0	9.3	65.9
12	34.1	17.5	79.9
13	43.0	15.0	103.1
14	46.0	19.7	102.3
15	25.9	9.0	58.8
16	37.5	13.8	73.4

Table 11 - Molten pool areas for the experiments of the second run

ID	FZ Inf Area (mm <sup>2</sup> )	FZ Sup Area (mm <sup>2</sup> )	HAZ Area (mm <sup>2</sup> )
17	7.0	7.2	13.1
18	8.7	8.9	15.1
19	5.9	7.4	9.8
20	7.9	5.9	14.2
21	8.5	6.9	16.9
22	8.0	6.9	17.8
23	8.8	7.5	20.8
24	11.3	10.1	23.3
25	8.5	3.8	20.5
26	11.8	7.2	29.8
27	10.5	8.1	25.4
28	12.4	9.5	34.1
29	12.0	8.9	29.8
30	11.6	7.2	29.4
31	14.0	9.2	36.9
32	13.3	9.0	33.1

In order to evaluate the dependency between the input variables and the results obtained by the experiments, were calculated the Determination Coefficient between the Heat Input and measured data. This coefficient measures the linear dependency between two variables and varies from 0 to 1. Zero means weak relation between the considered variables, while 1 means a strong linear relation. The main parameter that was assessed is the heat input, given by:

$$Heat\ Input = \frac{Power}{Travel\ Speed}$$

This parameter indicates the quantity of energy that is delivered per longitudinal length of welding. The heat input was divided into the part delivered by the laser welding and by GMAW. Was also considered the total heat input given by the sum of these two parts. The obtained values are given in Table 12.

Table 12 - Determination Coefficient ( $R^2$ ) between Heat Input and measured parameters

	Heat Input		
	Laser	GMAW	Total
Depth	0.866	0.573	0.850
Width	0.731	0.792	0.884
Inferior FZ Area	0.877	0.763	0.963
Superior FZ Area	0.566	0.884	0.813
HAZ Area	0.916	0.719	0.963

As expected, the first line of the table indicates that depth is mainly influenced by the laser welding. Although GMAW presents a much weaker relation with depth, some part of its generated heat may affect the bottom of the molten pool. For the width of the weld, may be expected that the GMAW is the principal influence. However, the coefficients show that laser and GMAW have an approximate contribution, being the total heat input the main impact.

Considering the inferior zone area, the total heat input was the one that presented the higher determination coefficient, very close to 1, indicating a strong relation with this part of the fusion zone. It is important to highlight that GMAW also presents some impact on the inferior fusion zone. On the superior fusion zone, the main influence is made by GMAW, as expected. This may be explained by the characteristic of the weld, which uses a filler material dropped on this zone. The last measured parameter, HAZ Area, is strongly influenced by the total heat input. Although laser also exerts a great effect on this parameter.

Microhardness test was carried out according to Section 2.2. In the top and the middle of the sample, we can observe a similar behaviour. In HAZ, hardness is significantly greater than PM. Such effect can be explained due to high thermal cycles during welding process. The thermal cycles rise up atomic diffusion inside and expand the grain size. Since cooling rate is high in arc welding, the hardenability of the materials grows up and favours the formation of martensite in this region. Then, hardness values are considerably higher at HAZ than in PM. At FZ, there was formation of dendrites that came out from solidification. These dendrites are slender and elongated grains and present high hardness values, as may be seen in Figure 13 and Figure 14.

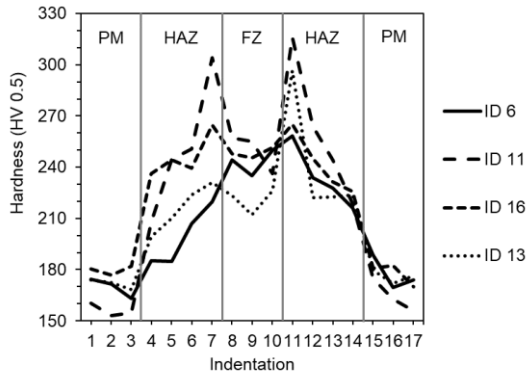


Figure 13 - Microhardness of KD 36 at PM, HAZ and FZ at the top

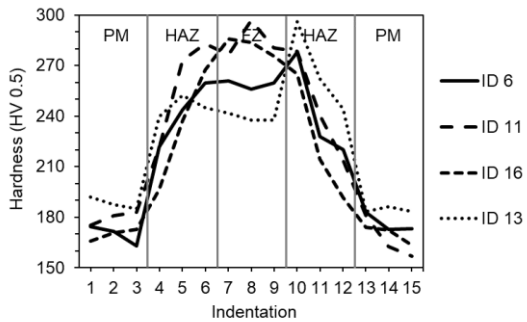


Figure 14 - Microhardness of KD 36 at PM, HAZ and FZ at the middle

#### 4.2. Simulation Results

Based on the heat sources adjusted earlier, it may be possible to compare the results between the combination of heat sources and the experiment. The first set of results is the shape of the fusion zone presented in Figure 15 and Figure 16. The first shows the contour of fusion zone generated by the combination of a cylindrical heat source for the laser beam welding and a double ellipsoid heat source for the GMAW. The second figure presents the same results for the second combination of heat sources, where a double ellipsoid heat source is used instead of the cylindrical for the laser beam. Both combinations of heat sources developed a good agreement with the shape of the fusion zone. Cylindrical combination missed a small part of fusion zone near the surface, where the GMAW is most acting. Differently, the double ellipsoid combination missed a small area at the bottom end of the fusion zone. This behaviour of double ellipsoid for deeper welds is expected, as it is not the best choice for this type of weld simulation. As presented, the cylindrical heat source had a better fit for this portion of the weld.

The second set of results is the comparison between the experiment and simulation residual stresses, shown in Figure 17. Analysing first the

transverse residual stresses, is possible to note that both combinations of heat sources generated a good prediction. Although the simulation overestimated the peak observed near the weld line, the major part of residual stresses had a good agreement with the experiment. Generally, transverse residual stresses are not well assessed by welding simulations, especially for small welded structures. Caprace (2017), observed differences around 35% for transverse residual stresses in comparisons between simulations and experiments. While longitudinal residual stresses presented differences around 18%.

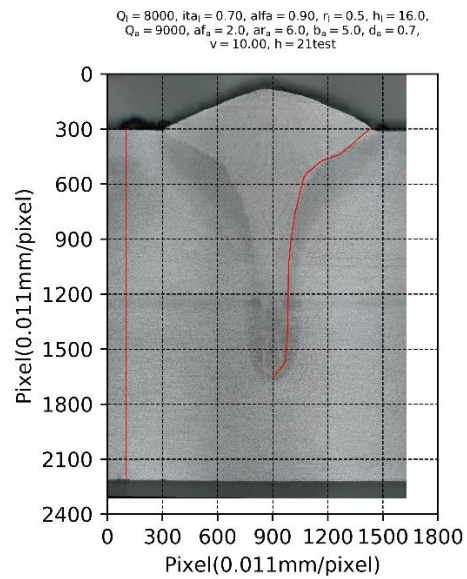


Figure 15 - Comparison of experiment and simulation fusion zone generate by cylindrical heat source

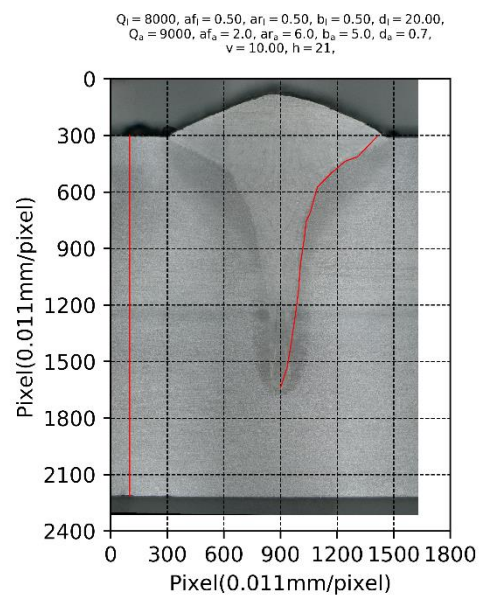


Figure 16 - Comparison of experiment and simulation fusion zone generate by double ellipsoid heat source

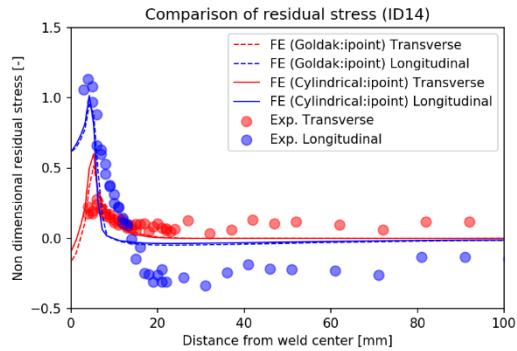


Figure 17 - Residual stress comparison between experiment and simulation

An opposite behaviour is observed for the longitudinal residual stresses, where the peak is well predicted by the simulations for both combinations of heat sources. However, simulations did not reach the same accuracy for the region out of the peak.

It is interesting that both combinations of heat sources generated a similar prediction for the transversal and longitudinal residual stresses. Even though small differences were observed on the temperature field exposed on the fusion zone (Figure 15 and Figure 16).

## 5. Conclusions

In this project, a set of welding experiments were developed in order to study the influence of inputs to the final weld bead. Moreover, a numerical simulation was made to assess the residual stresses generated by the welding hybrid process. The obtained results were compared to the experimental measures.

With the collected experimental data was possible to conclude that the depth of the weld bead is most affected by the laser input. For the width, laser and GMAW have an approximate influence. Although the total heat input is the main contribution.

Now considering the areas, inferior fusion zone is most affected by the total heat input. Even being the smaller influencer, GMAW has an important role in the size of this zone. On the superior fusion zone, GMAW is the most acting parameter. At least, for the HAZ area, the total heat input is the variable with a stronger relation. However, laser also affects significantly its size.

Considering the temperature field that defined the fusion zone, cylindrical combination had a better agreement for the laser beam welding. While double ellipsoid combination represented better the GMAW part of the fusion zone.

Hardness results presented a standard behavior. High cooling rate during welding triggered grains coarsening at HAZ and formation of dendrites at FZ, which characterizes a more fragile microstructure in these regions and raising hardness values related to PM.

From the residual stresses, it is important to highlight that for the chosen set of heat source parameters, the simulations achieved a good agreement with the experiment. The transversal residual stresses were well predicted for the most region of the experiment, overestimating its peak. While the peak was almost exact, the one observed for the longitudinal stresses. This may be an important result, which should be studied deeper. It may guide the reliability of the simulations for specific purposes.

Moreover, it may be concluded that the combination of heat sources was not a crucial decision for study. Both combinations resulted in similar predictions, as well for transversal as for longitudinal stresses.

## 6. References

- CAPRACE, JEAN-DAVID; FU, GUANGMING; CARRARA, JOICE F.; REMES, HEIKKI; SHIN, SANG BEOM. A Benchmark Study of Uncertainty in Welding Simulations. *Marine Structures*, vol. 56, pp.69-84, 2017.
- DERAKHSHAN, E. D.; YAZDIAN, N.; CRAFT, B.; SMITH, S.; KOVACEVIC, R. Numerical simulation and experimental validation of residual stress and welding distortion induced by laser-based welding processes of thin structural steel plates in butt joint configuration. *Opt Laser Technol*, Vol. 104, pp.170-82, 2018.
- DNV - DET NORSKE VERITAS. DNVGL-ST-F101 – Submarine Pipeline Systems. 2017.
- GOLDAK, J.; CHAKRAVARTI, A.; BIBBY, M. A New Finite Element Model for Welding Heat Sources. *Metallurgical Transactions B*, vol. 15B, pp. 299-305, 1984.
- KIM, YOU-CHUL; LEE, JAE-YIK; INOSE, KOUTAROU. The High Accurate Prediction of Welding Distortion Generated by Fillet Welding. *Quarterly Journal of the Japan Welding Society*, Vol. 23, Issue 3, pp.431-435, 2005.
- KONG, Fanrong; MA, Junjie; KOVACEVIC, Radovan. Numerical and experimental study of thermally induced residual stress in the hybrid laser-GMA

welding process. *Journal of Materials Processing Technology*, pp.1102-1111, 2011.

MASATO, MOCHIZUKI; SAITO, NAOTO; ENOMOTO, KUNIO; SAKATA, SHINJI; SAITO, HIDEYO. Study on Internal Residual Stress of Multi-Pass Butt-Welded Plate Joint Using Inherent Strain Analysis. *Transactions of the Japan Society of Mechanical Engineers Series A*, Vol. 64, Issue 587, pp.1568-1573, 1995.

PAN, Qinglong; MIZUTANI, Masami; KAWAHITO, Yousuke; KATAYAMA, Seiji. Effect of shielding gas on laser-MAG arc hybrid welding results of thick high-tensile-strength steel plates. *Welding in the World*, pp.653-664, 2016.

PARDO, E.; WECKMAN, D. C. Prediction of weld pool and reinforcement dimensions of GMA welds using a finite-element model. *Metallurgical Transactions B*, Vol. 20, Issue 6, pp.937-947, 1989.

PASTERNAK, H.; LAUNERT, B.; KANNENGIEBER, T.; RHODE, M. Advanced Residual Stress Assessment of Plate Girders Through Welding Simulation. *Procedia Eng*, Vol. 172, pp23-30, 2017.

WAHBA, M.; MIZUTANI, M.; KATAYAMA, S. Single pass hybrid laser-arc welding of 25 mm thick square groove butt joints. *Materials & Design*, pp.1-6, 2016

XIA, J.; JIN, H. Analysis of residual stresses and variation mechanism in dissimilar girth welded joints between tubular structures and steel castings. *Int J Press Vessel Pip*, Vol. 165, pp.104-113, 2018.